01 Jan 2005

Aircraft Cabin Noise Minimization Via Neural Network Inverse Model

Xiao Hu

G. Clark

M. Travis

J. L. Vian

et. al. For a complete list of authors, see https://scholarsmine.mst.edu/ele_comeng_facwork/857

Recommended Citation

X. Hu et al., "Aircraft Cabin Noise Minimization Via Neural Network Inverse Model," *Proceedings of the IEEE International Joint Conference on Neural Networks, 2005*, Institute of Electrical and Electronics Engineers (IEEE), Jan 2005.
The definitive version is available at https://doi.org/10.1109/IJCNN.2005.1556267

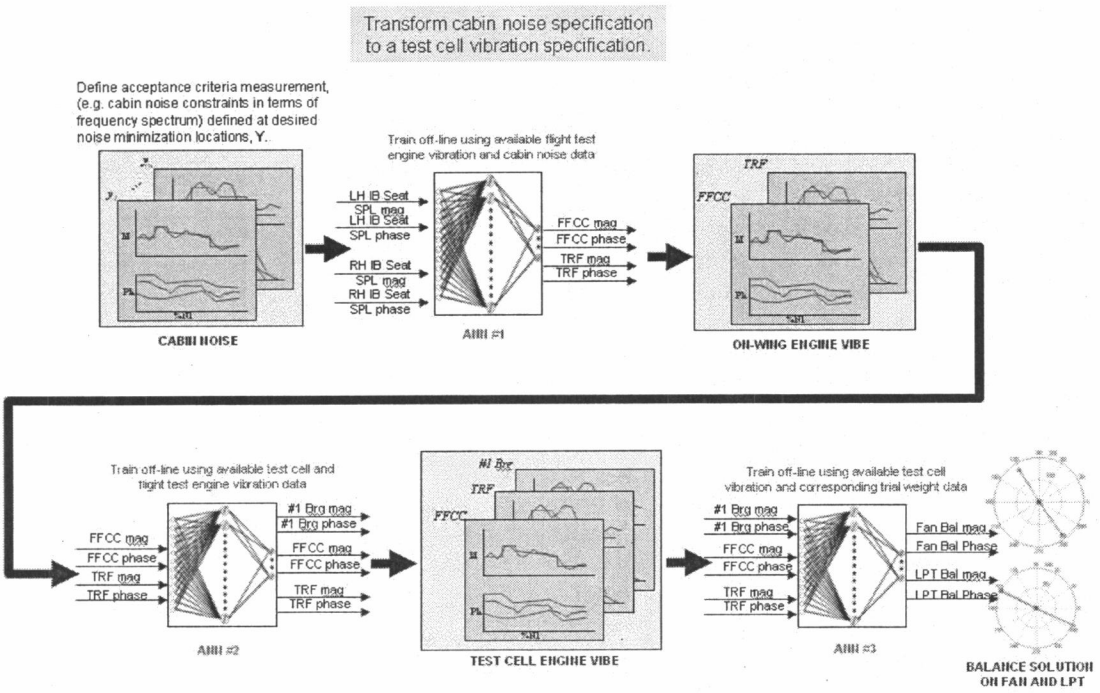

Figure 3. The detailed neural network inverse model, which maps from cabin noise specification to engine balancing solution. The ANN #1 is used to learn the relationship from cabin noise to on-wing, in-flight vibration. The ANN #2 is used to learn the relationship from on-wing, in-flight vibration to test-stand vibration. At last, the ANN #3 is used to learn the relationship from test-stand vibration to trial weights. Each network is trained separately.

bins) and 24(4 components × 6 frequency bins) for ANN #1, 24 (4 components × 6 frequency bins) and 36 (6 components × 6 frequency bins) for ANN #2, 36 (6 components × 6 frequency bins) and 4 for ANN #3. According to [4], those amplitude and phase representation are all converted into real and imaginary representation before being presented to the networks for training.

The generated datasets are divided into two parts, a training set and a validation set, which is used to prevent network overfitting. Each network is set up as multilayer perceptrons (MLP) and trained by the Levenberg-Marquardt algorithm [7]. At the end of training, a zero vector (24-by-1), which corresponds to zero cabin noise on the LHS and RHS, is presented to ANN #1 as an input. It is fed through the ANN #1, ANN #2 and ANN #3 to come up with a solution to balance the fan and LPT on the engine. This balance solution is supposed to be the trial weights to generate the corresponding zero cabin noise. However, this proved to be NOT the case.

C. Validation

Different network setups are tried and different training algorithms are employed, but the inverse model always generate different balance solutions with large variance in terms of different amplitude and phase angle at every run of network training. When those balance solutions are put on back the engine, their corresponding cabin noise can be computed by IC_{cabin} in the same way described in the data generation section. The resulting cabin noise is not necessarily lower than the as-is cabin noise but mostly higher, which obviously shows that there is something unusual with either the model or the data. To demonstrate the validity of the neural network inverse model, instead of having a zero vector to ANN #1 as input, the as-is cabin noise is presented. If the neural network inverse model works properly in terms of finding the mapping from in-flight cabin noise to test-stand vibration, and further to trial weights, it should produce zero balancing solution from ANN #3 apparently, which means no trial weight should be added on the engine to get the as-is cabin noise. The experiment shows it does perform as expected. This also proves that the neural network inverse model is correct. When Equation (1) and (2) are re-examined, it is realized that, to make the assumption of system linearity valid, the IC matrix $R(f)$ has to be the same as the $R_{asis}(f)$ in Equation (3):

$$X_{asis}(f) = R_{asis}(f)F_{asis} . \quad (3)$$

So in Equation (2), it can be expressed as follows:

$$X'(f) = (X_{asis}(f) + \Delta X(f)) = R_{asis}(f)F_{asis} + R(f)\Delta F = R(f)F . \quad (4)$$

But this is not generally true in reality. To prove this, the known $IC_{testcell}$ is inversed and then used together with the known as-is test-stand vibe data to compute the residual mass unbalance on the engine, as shown in equation (5):

$$F_{asis}=(R_{asis}(f))^{-1} X_{asis}(f) . \quad (5)$$

If the assumption of system linearity holds, the residual mass unbalance should be the same across the frequency spectrum. But this simple computation based on equation (5) shows the inconsistence of computed residual unbalance, which demonstrates the difference between the as-is IC matrix $R_{asis}(f)$ and the IC matrix $R(f)$ computed by the two-plane engine balancing approach. This difference brings confusions into the generated data, which makes it very difficult for the neural network inverse model to discover the true correlation between cabin noise and test-stand vibration. It is also demonstrated that more real test cell and flight test data are needed directly to investigate the relationship between test-stand vibration and cabin noise.

III. THE MODELING ON THE DATA FROM EMPIRICAL MODELS

Although more real data are needed to look into the true relationship between cabin noise and test-stand vibration, it is believed that neural network inverse models can play an important role in unraveling this relationship. In the proof-of-concept experiments for the neural network inverse model's effectivity in cabin noise minimization problem, more data are generated by empirical engine/airplane models to see if the neural network model can correctly discover the relationship from the data. Actually, the data generated from the empirical engine/airplane models can be obtained from ongoing data-collection processes if necessary.

A. Data Generation

It has been shown that the problem of modeling on the real test data lies in the inconsistence of IC matrix between the $R(f)$ computed by two-plane balancing approach and the $R_{asis}(f)$. To avoid this, the $R_{asis}(f)$ is forced to be equal to $R(f)$ in the empirical model. In other words, given known residual mass unbalance on engine, the $IC_{testcell}$, IC_{onwing} and IC_{cabin} which are computed as in Section II.A, are used as as-is IC matrices to generate as-is responses for test-stand vibration, on-wing vibration, and cabin noise. Except for this difference, the way that the data were generated was the same as described in section 2.1. To test the robustness of the neural network inverse model, seven cases with different residual mass unbalances on the fan and LPT are tried. In the experiments, the inverse model method is proved valid in all these different cases. Also, the trial weights are applied on the empirical IC models to generate simulated data.

	Fan – residual		LPT – residual	
	Amount (g/cm)	Angle (deg)	Amount (g/cm)	Angle (deg)
Case 0	558	70	309	250
Case 1	237	140	0	0
Case 2	480	210	0	0
Case 3	184	305	492	154
Case 4	769	255	309	247
Case 5	558	65	170	225
Case 6	1117	230	309	285

Table 1. Residual mass unbalances in the 7 cases.

B. Modeling

The same inverse model as shown in Figure 3 can be applied on the data from the empirical models to look into the relationship between test-stand vibe and cabin noise. The data are also divided into training and validation sets to prevent overfitting, as in section II.B. Each network is set up as multilayer perceptrons (MLP) and trained by the Levenberg-Marquardt algorithm. At the end of training, a zero vector (24-by-1), which corresponds to zero cabin noise on LHS and RHS, is presented to ANN #1 as input. It is fed through ANN #1, ANN #2 and ANN #3 to come up with a solution to balance Fan and LPT. This balance solution is supposed to be the trial weights, which should be put on the engine to generate the corresponding zero cabin noise. The experimental results are shown in section III.C.

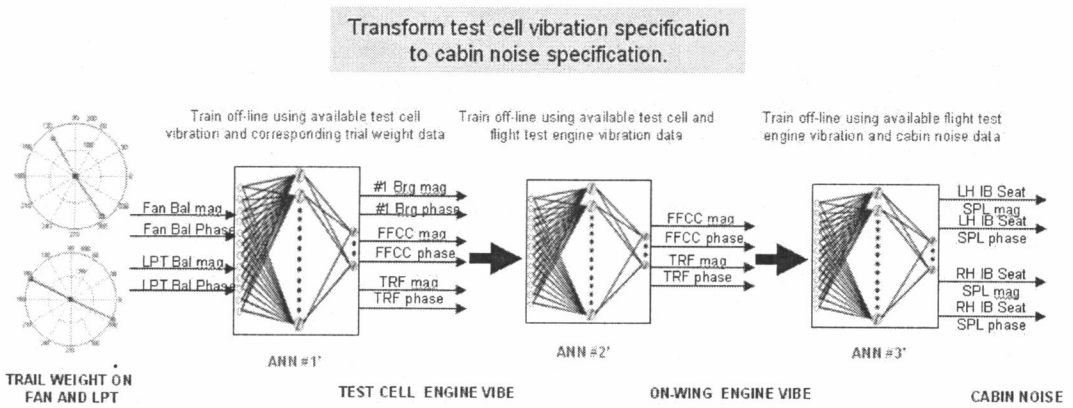

Figure 4. The neural network model in the opposite direction to the model in Figure 3.

Another neural network model is constructed in the opposite direction to the model in Figure 3. It is shown in Figure 4, which uses ANN #1' to learn from trial weight on-engine to test-stand vibe, uses ANN #2' to learn from test-stand vibe to engine vibe on-wing and uses ANN #3' to learn from engine vibe on-wing to cabin noise in flight. Each network is trained separately. At the end of training, it would be interesting to present the balancing solution from the model in Figure 3 to ANN #1' as input to see if ANN #3' can come up with the output of a zero vector, which corresponds to the zero cabin noise. This way, the functional mapping between cabin noise and test-stand engine vibe can be proved to exist in both directions. The experimental results are shown in section III.C.

C. Experimental Results

The neural network inverse model using ANN #1, ANN #2 and ANN #3 is set up as multilayer perceptrons. Same as described in section II.B, the dimensions of input vector and output vector in each neural network are respectively, 24×1 and 24×1 for ANN #1, 24×1 and 36×1 for ANN #2, 36×1 and 4×1 for ANN #3. All the complex data are expressed in the format of real and imaginary. After some trials, the network architect is selected as 15-24, 15-36 and 18-4 for ANN #1, #2 and #3, respectively. The transfer functions of the hidden layer and output layer are sigmoid and linear. Each network is trained separately using the Levenberg-Marquardt algorithm, which is shown to be faster than other backpropagation variants. During the course of training, the performance on validation set is monitored for the early stopping of training in order to prevent overfitting. At the end of training, a zero vector, which corresponds to zero cabin noise on the LHS and RHS, is presented to ANN #1 as input. It is fed through ANN #1, ANN #2 and ANN #3 to come up with a solution ΔF to balance Fan and LPT. Putting the ΔF back on the engine, a nearly zero (if not zero) cabin noise should be returned based on Equation (6) as:

$$X' = IC_{cabin}F' = IC_{cabin}(F_{asis} + \Delta F), \qquad (6)$$

if the modeling is correct. Figure 5 shows the results of the balancing solution and the comparison of the cabin noise before/after the engine is balanced from ten runs of network training with a random initial state. In the Figure 5(a), the amount and the angular position of the balancing weight is indicated by the red square, while the residual mass unbalance is represented by the blue asterisk. In the Figure 5(b)(c), the vibration/noise before and after the engine is balanced are represented by the red dashed line and the blue solid line, respectively. Clearly, the average of the results accurately estimates the mass unbalance on the engine and the test cell vibration and the cabin noise are reduced dramatically after the engine is balanced. The neural network inverse model is also proved valid on all the other unbalance cases.

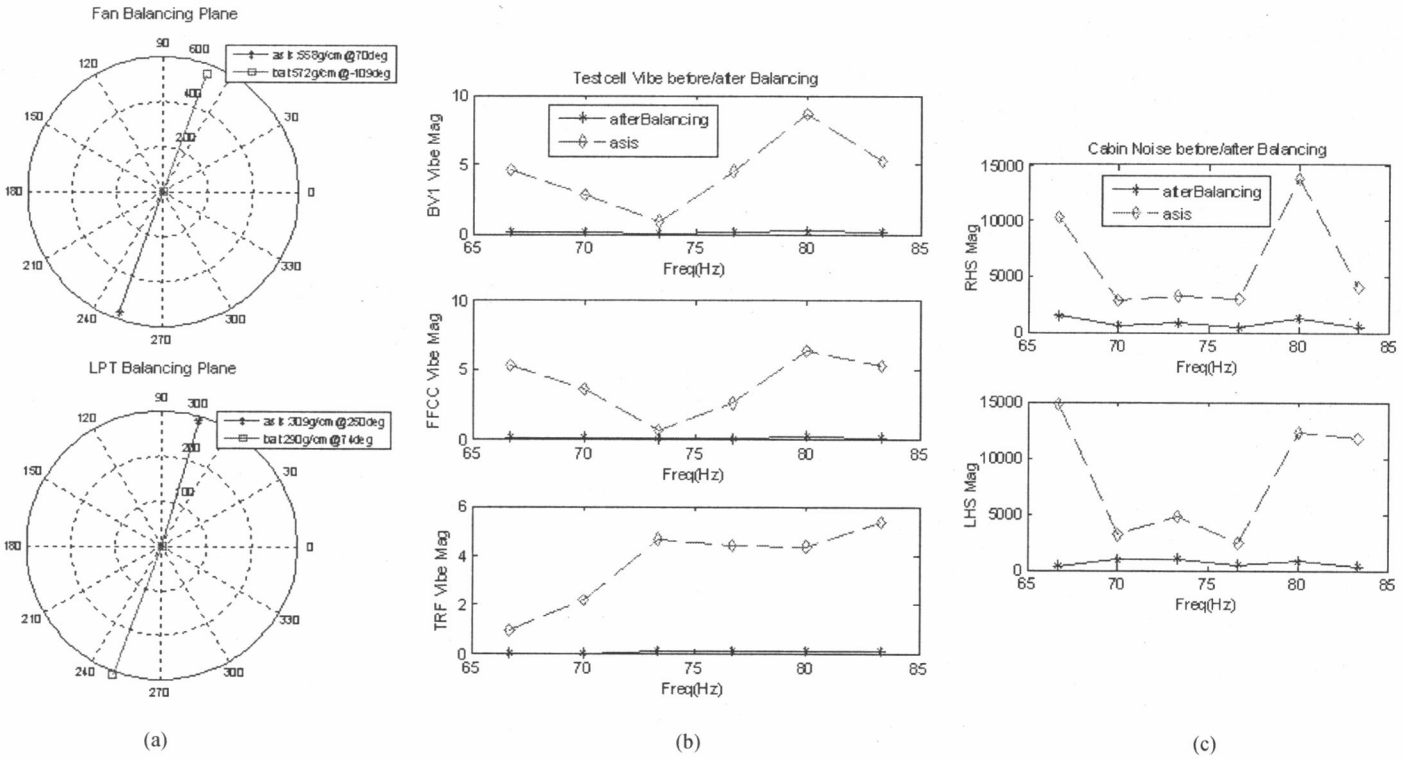

Figure 5. The results on unbalancing Case 0. (a) Residual Unbalance & Balancing Solution on Fan and LPT; (b) Test-stand Vibe Response before/after Balancing; (c) Cabin Noise before/after Balancing.

The neural network model shown in Figure 4 is trained with the same datasets used in the inverse model (see Figure 3). The input and output of ANN #1', #2' and #3' are the output and input of ANN #3, #2 and #1, accordingly. After some trials, the network architect is selected as 4-36, 15-24 and 15-24 for ANN #1', #2' and #3', respectively. The transfer functions of the first hidden layer and output layer were sigmoid and linear, respectively. Each network is trained separately using the Levenberg-Marquardt algorithm. At the end of training, the balancing solution generated from the previous neural network inverse model (ANN #1, #2 and #3) is presented to ANN #1' as input to be fed through the network model. By doing so, the ANN #1' and 3' produced the similar test-stand vibration response and cabin noise as the results generated by Equation (6). This proves that the validity of the neural network inverse model by showing the feasibility of the modeling from both directions of data mapping paths.

IV. CONCLUSIONS

A new neural network approach is developed and shown to be able to accurately model the relationships between engine unbalance and vibration/noise to overcome limitations associated with traditional linear influence coefficient methods. This report illustrates the limitations of the traditional methods, and shows that the ANN methods are able to account for them and thus provide more accurate model representations. The methods are used to determine test-stand or on-wing balance solutions to satisfy cabin noise specifications. The accuracy of the ANN model with respect to the real system is determined by the quantity of experimental data made available from test stands and/or operational aircraft. Thus, ongoing processes to capture this data will be required to ensure sufficient data is available to facilitate successful implementation. Although this paper is contributed to minimize in-flight cabin noise, the techniques applied can be easily adapted to accommodate vibration data from actual propulsion systems to the diagnosis of the health conditions of other system components.

ACKNOWLEDGEMENT

Partial support for this research from the Boeing Company, the National Science Foundation, and from the M.K. Finley Missouri endowment, is gratefully acknowledged.

REFERENCES

[1] J.L. White, M.A. Heidari, M.H. Travis, "Experience in Rotor Balancing of Large Commercial Jet Engines," SEM, Proceedings of the 13th Intl Modal Analysis Conf., Vol II, 1995, pp. 1338-1344.

[2] X. Hu, J. Vian, J. Choi, D. Carlson, D.C. Wunsch II, "Propulsion Vibration Analysis Using Neural Network Inverse Modeling," Neural Networks, Proceedings of the IJCNN'02 International Joint Conference on, vol.3, pp. 2866 –2871, 2002.

[3] X. Hu, J. Slepski, J. Vian, D.C. Wunsch II, "Vibration Analysis Via Neural Network Inverse Models To Determine Aircraft Engine Unbalance Condition," Neural Networks, Proceedings of the IJCNN'03 International Joint Conference on, vol.4, pp.3001-3006, 2003.

[4] X. Hu, M. Travis, J. Vian, D.C. Wunsch II, "Aircraft Engine Balancing Using Neural Network Inverse Model," Technical Report, Boeing Phantom Work, August, 2003.

[5] J.L. White, S.A. Shipley, T.F. Yantis, "Active Control Studies of Structurally Transmitted Engine Vibration on Commercial Airplanes," Proceedings of the 12th Intl Modal Analysis Conf., January, 1994.

[6] J.L. White, M.A. Heidari, T.F. Yantis, "A Study of Engine Excited Non-linear Vibro-acoustics in Commerical Airplanes," Proceedings of 15th International Model Analysis Conference, p.1503, 1997.

[7] Simon Haykin, Neural Networks: a comprehensive foundation, 2nd Ed., Prentice Hall, New Jersey, 1999.

[8] T. Brotherton, G. Chadderdon, P. Grabill, "Automated Rule Extraction for Engine Vibration Analysis," Proceedings of IEEE Aerospace Conference, vol. 3, pp. 29 –38, 1999.

[9] A.C. McCormick, A.K. Nandi, "Real-Time Classification of Rotating Shaft Loading Conditions Using Artificial Neural Networks," IEEE Trans. On Neural Networks, Vol. 8, No.3, pp. 748 - 757 , May, 1997.

[10] J. T. Renwick, "Vibration Analysis – A Proven Technique as A Predictive Maintenance Tool," IEEE Trans. Ind. Applicat., vol. 21, pp. 324-332, Mar, 1985.

[11] J. S. Mitchell. An Introduction to Machinery Analysis and Monitoring – 2nd ed. PennWell Publ. Comp. 1993.

[12] R. R. Schoen et al., "An Unsupervised, On-line System for Induction Motor Fault Detection using Stator Current Monitoring", IEEE Trans. Ind. Applicat., vol. 31, no. 6, pp. 1274-1279, 1995.

[13] T. I. Lui, J.M. Mengel, "Intelligent Monitoring for Ball Bearing Conditions", Mech. Syst. Signal Processing, vol. 6, no. 5, pp. 419-431, Sept., 1992.

[14] C. K. Mechefske, J. Mathew, "Fault Detection and Diagnosis in Low-speed Rolling Element Bearings Part I: The Use of Nearest Neighbor Classification", Mech. Syst. Signal Processing, vol. 6, no. 4, pp. 297-307, July, 1992.

Dynamic Neural Network-based Estimator for Fault Diagnosis in Reaction Wheel Actuator of Satellite Attitude Control System

Ehsan Sobhani Tehrani & K. Khorasani
{e_sobhan,kash}@ece.concordia.ca
Department of Electrical & Computer Engineering
Concordia University, Montreal, Quebec, H3G 1M8 CANADA

S. Tafazoli
Canadian Space Agency
6756, route de l'Aeroport
Saint-Huber, Quebec, J3Y 8Y9 CANADA

Abstract-This paper presents an approach to simultaneous fault detection and isolation in the reaction wheel actuator of the satellite attitude control system. A model-based adaptive nonlinear parameter estimation technique is used based on a highly accurate reaction wheel dynamical model while each parameter is an indication of a specific type of fault in the system. The estimation is based on the nonlinear finite-memory filtering strategy that is solved for optimal estimation functions. To make the optimization feasible for on-line application, the optimal estimation functions are approximated by MLP neural networks thus reducing the functional optimization problem to a nonlinear programming problem, namely, the optimization of the neural weights. The well-known standard back-propagation algorithm and back-propagation through-time algorithm were employed inside the neural adaptation algorithms to obtain the required gradients. Simulation results show the effectiveness of the methodology for the proposed application.

I. INTRODUCTION

There is an increasing demand for man-made dynamical systems to operate autonomously in presence of faults and failures in sensors, actuators or components. These requirements are of particular importance to systems such as highly advanced satellites and space probes. As satellites become more complex and autonomous, on-board diagnosis functions and capabilities grows in importance. In the literature a system that is capable of *detecting, isolating, recovering* faults is known as an FDIR system. The FDIR system should be capable of detecting and isolating various types of faults including multiple faults that may happen at the same time in different components or subsystems of a satellite including the attitude determination and control subsystem (ADCS). The ADCS subsystem stabilizes the satellite and orients it in desired directions even in the presence of external disturbances acting on it. The actuator that is basically used in today's satellites for active attitude alteration is the reaction wheel which produces and applies corrective torques on the satellite's body. In this paper, we will not address the fault recovery problem, therefore we make the assumption that the control input $u(t)$ and the state vector $x(t)$ remain bounded prior to and after the occurrence of a fault.

As model-based fault diagnosis and isolation (FDI) techniques are based upon the mathematical model of the system, modeling uncertainties and process noise and disturbances will affect the performance of the FDI unit leading to missed and false alarms. Therefore, it is an important requirement to have a highly accurate analytical model of the reaction wheel dynamics and disturbances. This is our motivation in section 2 where a detailed nonlinear mathematical model of the reaction wheel in conjunction with the attitude dynamics of the satellite is presented.

During the last two decades a number of works have been developed using model-based analytical approaches to FDIR. These techniques may be divided into three basic approaches: observers [1], parameter estimation [3,4], and parity equations [2]. Although the work presented in this paper is different from the parameter estimation approach proposed in [3,4], we conceptually follow the same general idea. The difference basically originates from the manner we define the parameters that need to be estimated. Here we make use of the fact that sensor, actuator, or component faults of a dynamic system can be reflected in a set of parameters designated as *fault parameters* which affect the physical parameters of the system in additive or multiplicative forms. Faults are then detected by estimating these fault parameters and comparing the estimates with the parameter values under healthy conditions. It should be noted that in contrast in the standard parameter estimation approaches the plant parameters themselves have to also be estimated.

State and parameter estimation under the assumption of linearized system dynamics and Gaussian process and measurement noises can be accomplished optimally using Kalman filter [6]. For nonlinear systems, however, it is well-known that the nonlinear extension of the Kalman filter called Extended Kalman Filter (EKF) suffers greatly from divergence due to modeling errors and disturbances. To overcome this drawback [7,8] originally proposed the finite-memory estimation for nonlinear systems. Finite-memory estimation is based on the idea that the data older than a given number of time steps will not influence the current estimate. Again under the linear-Gaussian assumptions, the analytical solutions exist for the estimation laws while for nonlinear

0-7803-9048-2/05/$20.00 ©2005 IEEE

systems approximations are required. In [9] finite-memory estimation has been applied to the problem of fault detection in linear continuous-time systems. For the application of finite-memory estimation to identification problems see [10].

Neural networks are basically an important class of on-line approximators due to their on-line learning capabilities, their universal approximation property, and the distributed nature of their parameters (or weights). The use of neural networks in fault diagnosis is basically based on their ability to model nonlinear dynamic systems. In this regard, [5] have presented the general fault diagnosis scheme as shown in fig. 1 where each fault model in the residual generation block is a *dynamic neural network* that identifies a class of system behavior. In the decision making stage another neural network is used for the purpose of residual evaluation based on the *classification* capability of neural networks. For a detailed discussion on different network architectures and algorithms that have been deployed in this general framework see the survey paper of [5].

In this paper, we are not adopting the above general architecture. Instead, the FDI problem will be formulated as an on-line nonlinear parameter and state estimation problem where the nonlinear functions in the solution of the estimation problem will be approximated by using neural networks of the MLP (Multi-Layer Perceptron) architecture. Whenever needed, dynamics will be introduced to the MLP networks using tapped delay line operator in the feedback loop.

II. Reaction Wheel Model and Attitude Dynamics

Reaction wheels are moment exchange devices that provide reaction torque to a satellite body and store angular momentum used for the purpose of active and passive attitude control, respectively. It consists of a rotating flywheel driven by an internal brushless DC motor. The only input to the reaction wheel is a torque command (voltage) which controls motor current and consequently the motor torque. Based on the Newton's third law of motion, the reaction torque applied to the satellite body is equal to and opposite to the net torque that accelerates and decelerates the flywheel. The detailed mathematical model of the reaction wheel, in block diagram form, is given in Fig. 2 which includes nonlinearities as well as internal disturbances that are present in a real system [11,12]. In this figure the gain K_t is the motor torque constant which delivers torque proportional to the current I_m which itself is directly proportional to the torque command voltage, G_d is the gain of the motor driver which is essentially a voltage controlled current source. A speed limiter circuit is applied to keep the speed of the flywheel in the safe range specified by the threshold ω_s. A high-gain negative feedback k_s will be provided into the command torque whenever the threshold is exceeded.

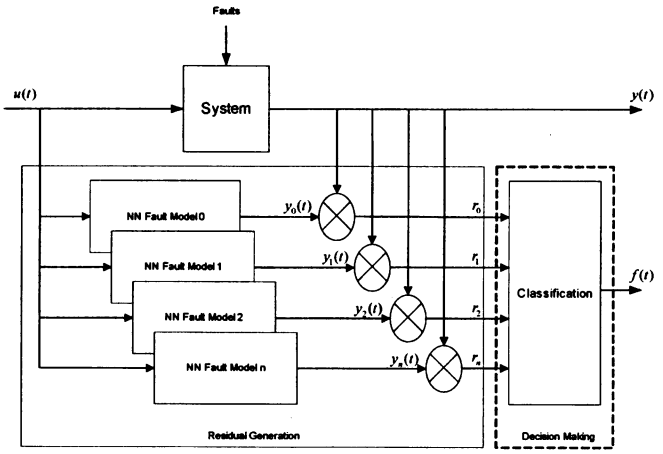

Fig. 1. General Fault Diagnosis Scheme with Neural Networks [5]

The increase of back-EMF, k_e, of the motor at high speeds may limit the motor torque specifically at low bus voltage conditions. The back-EMF limiting is also mildly coupled to power consumption through voltage drops in the input filter due to the product of the bus current, I_{BUS}, and the input filter resistance, R_{IN} where I_{BUS} is a highly nonlinear function of the states, I_m and ω, and the bus voltage, V_{BUS}.

In case no power is being drawn from the bus, for instance during deceleration, the heavy-side function, H_b, eliminates the voltage drop. In addition, a reverse polarity protection diode drop of 1V is also modeled by H_b. The friction effect is mathematically broken down into viscous friction, modeled by the speed and temperature dependent factor τ_v, and coulomb friction, modeled by a constant, τ_m, with polarity dependence on wheel direction of rotation. Torque noise, a very low frequency torque variation from the bearings due to lubricant dynamics, is also modeled. The torque motor in a reaction wheel can be a source of very high frequency disturbances due to the motor excitation and the magnetic construction which is modeled as cogging and torque ripple frequency varying sinusoidal signals in a feedback loop with frequencies depending on the number of poles of the DC motor and the motor speed.

For the reasons that will be clarified later in section 4, we approximate all the discontinuous blocks in the reaction wheel model by continuous differentiable functions. These functions represented by $\psi_1, \psi_2, \text{and} \psi_3$, are approximating EMF torque limiting, coulomb friction, and speed limiter subsystems, respectively. For notational simplicity torque ripple and cogging are represented by φ_1 and φ_2, respectively. The closed-form nonlinear state-space representation of the reaction wheel model may be expressed as follows:

$$\begin{bmatrix} \dot{I}_m \\ \dot{\omega} \end{bmatrix} = \begin{bmatrix} G_d\omega_d[\psi_1(I_m,\omega)-\psi_3(\omega)]-\omega_d I_m \\ \frac{1}{J}[K_t I_m(1+B\varphi_1(\omega,t))-\tau_c\psi_2(\omega)-\tau_v\omega+C\varphi_2(\omega,t)] \end{bmatrix} + \begin{bmatrix} G_d\omega_d \\ 0 \end{bmatrix} V_{\text{Com}}$$

$$y=\omega=[0 \;\; 1]\begin{bmatrix} I_m \\ \omega \end{bmatrix} \qquad (1)$$